Cloud Publications
International Journal of Advanced Remote Sensing and GIS
2016, Volume 5, Issue 3, pp. 1618-1638
ISSN 2320 - 0243, Crossref: 10.23953/cloud.ijarsg.48

Research Article | Open Access

Spatial Variability of Urban Heat Islands in Cairo City, Egypt using Time Series of Landsat Satellite Images

Islam Abou El-Magd[*1], Ahmed Ismail[2] and Naglaa Zanaty[1]

[1]Environmental Studies Department, National Authority for Remote Sensing & Space Sciences Cairo, Egypt
[2]Environmental Science Department, Faculty of Science, Port Said University, Port Said, Egypt

Publication Date: 14 March 2016

DOI: https://doi.org/10.23953/cloud.ijarsg.48

Abstract Global warming has obtained more attention because of increasing global mean surface temperature since the late 19th century. Urbanization is considered an important contributor to global warming in big cities. Cairo is one of the heavily populated cities in the world, which has rapid urbanization that resulted in remarkable temperature variation compared to the rural surrounding areas. This phenomenon is known as "Urban Heat Islands" (UHIs) that influence both local and regional climate, environment, and socio-economic development. In this research time series of satellite images were used to map the spatial variability of Land Surface Temperature (LST) and Heat Islands in Cairo city. Historical and contemporary record of Landsat images nearly 16 dates from 1990 to 2014 were used to retrieve LST and land cover categories. Results showed that LST was highly influenced by Land use and land cover changes; heat island effect was dominant in urbanized areas, bare/desert land and industrial zones (e.g. Shobra El-khema). The industrial zones, in particular, were possibly high due to the aluminum roof material plus the thermal energy from production activities and high emissions of air pollutants. The pattern of spatial distribution of heat islands has significantly changed from bare/desert land and built up areas (as warmer) to cultivated land and water bodies (as colder). To analyze the relationship between Heat Islands and land-cover changes a quantitative correlation between LST and Normalized Difference Vegetation Index (NDVI), Modified Normalized Difference Water Index (MNDWI) and Normalized Difference Build-up Index (NDBI) was employed. It was found that the correlation between LST and NDVI and MNDWI was negative with r^2 of 0.8 and 0.57 respectively; however, the correlation with NDBI was strongly positive with r^2 of 0.81. It is anticipated that the outcomes of this research will contribute to GEOSS for global integration and correlation.

Keywords *Remote Sensing; Land Surface Temperature; Mono Window Algorithm; Cairo*

1. Introduction

Global warming phenomenon has obtained more attention due to the recognized increase of the global mean surface temperature since the late 19th century. Urbanization is considered an important contributor to global warming in cities. Generally, the rapid population growth and urban expansion, to

meet such population, with dense urban infrastructure have significantly affected the quality of life of urban inhabitants and negatively changed the urban environment and climate [1, 2]. This has introduced the phenomenon of Urban Heat Islands (UHIs) that was first documented by Howard [3]. Since that time it has been studied in many cities around the world. Simply, this phenomenon is described as the alteration of temperatures in urban areas compared to their rural surroundings [4]. Throughout the last decade, heat islands have been observed and examined in many cities around the globe such as Lódz, Poland [5], Athens, Greece [6], Beijing, China [7], Hong Kong, China [8], Shanghai, China [9], Glasgow, UK [10], Leipzig, Germany [11], Nagoya city, Japan [12], in some Asian mega cities including Tokyo, Beijing, Seoul, Shanghai, Pyongyang, Bangkok, Manila and Ho Chi Minh City [13], the largest cities of Greece (Athens, Thessaloniki, Volos, Patra and Heraklion) [2], in addition to a total of 263 European cities were studied by [4].

Generally, UHIs in cities depend mainly on the size, population and industrial development of a city, topography, physical layout, regional climate and meteorological conditions [14]. Therefore, many factors are influencing the formation of the urban heat islands that includes a) construction materials of high heat capacity and low solar reflectivity (e.g. asphalt and concrete), b) reduced turbulent heat transfer and long-wave radiative heat loss due to street canyons geometry, c) reduced latent heat loss by evaporation due to the replacement of the natural green surfaces with dry surfaces and, d) increased anthropogenic heat emissions into the urban atmosphere [2].

Traditionally, urban heat islands could be recorded by measuring air temperature through the use of automobile transects and weather station networks. However, recently with the advancement of the remote sensing sensors, remote sensing used to measure the surface temperature [15, 16, 17, 18, 19, 20, 21]. Surface temperature is the cumulative effects of surface radiative and thermodynamic properties including surface moisture, surface emissivity, surface albedo, their radiative input at the surface, and the effects of the near surface atmosphere, in addition to the turbulent transfer from the surface [22]. It has strong relation with the changes of the land cover patterns especially changes associated with the urban expansion [23]. It has found that land surface temperature has direct link with the biophysical, such as built-up area and height [24], urban and street geometry [25], land use and land cover [17], vegetation [21], as well as population density and distribution [26, 27, 28] and the intensity of human activities [29].

The purpose of this study is to analyze the spatial variability of urban heat islands in Cairo as one of the highest populated cities in the world using time series of Landsat data in the last 24 years. It will also examine the changes of the pattern of land use and land cover to investigate the impact of such changes on the intensity and spatial pattern of the UHIs. This will enable to examine and understand the relationship between urban heat islands and the key bio-physical drivers in the city.

Area of Study

Cairo is the capital of the Arab Republic of Egypt and is one of the largest cities in Africa and the Middle East [30]. It is considered an important political and cultural focal point in the region. Geographically, it is located on the Nile River at the southernmost tip of the Nile delta nearly 165 km south of the Mediterranean Sea and 120 km to the west of the Gulf of Suez and Suez Canal [31, 32]. Figure 1 shows the location map of the study area and the administrative boundary of Cairo city in alignment with the surrounding governorates. Where the selected study area extends from 29°56′N, 31°10′E to 30°12′N, 31°29′E; including Cairo city, parts of Al-Giza and Al-Qalyubia Governorates, extends from Al-Obour city and Qalyob district at north to Al-Giza district and New Cairo city at south. The Nile River is located in the western part of the study area.

Cairo has a hot dry climate with limited rainfall and often high humidity due to the effects of the Nile River and its valley. The mean air temperature in Cairo ranges from 9°C to 24.8°C in the winter and

from 20.1°C to 34.7°C in the summer and may surpass more than 40°C in some hot days (analysis of the WMO – World Meteorological Organization- data from 1971-2000).

Cairo is a densely populated city due to the rapid increase in urbanization and population in the last few decades [33]. Its population count increased from 5,466,742 people in 1986 to 6,000,716 people in 1996 and 6,758,581 people in 2006 according to CAPMAS (Central Agency for Public Mobilization and Statistics) census data. In 2006 CAPMAS has estimated the projected population count of Cairo would be about 9,102,232 people in 2014. This in addition to about 10 million inhabitants just on the margin of the city and they have a daily interaction with the city.

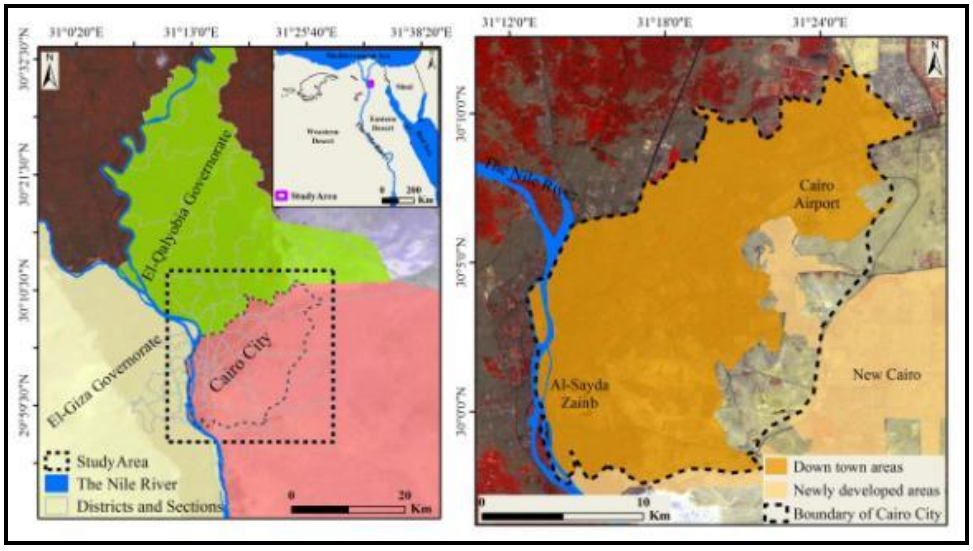

Figure 1: *Area of Study – Cairo City*

2. Materials and Methods

2.1. Satellite Data

In this research Landsat satellite data (i.e. Landsat TM/ ETM+ and Landsat8) was used in the last 24 years (from 1990 to 2014). The data is downloaded from the US Geological Survey (USGS) website (http://glovis.usgs.gov/) (Path 176 and Row 39). 16 dates were mainly downloaded to cover summer time (12 dates – July-August) and winter time (4 dates – December-January). Table 1 lists the sensor type and corresponding captured dates.

Table 1: *List of the Landsat Data Used*

Sensor Type	Acquisition Date	Acquisition Hour	Season
LandSat5 TM	04 Aug. 1990	07:43:51	Summer
	13 Aug. 1999	08:01:29	Summer
	07 Jul. 2003	08:00:08	Summer
LandSat7 ETM+	23 Aug. 2000	08:14:51	Summer
	30 Jan. 2001	08:14:21	Winter
	19 Dec. 2002	08:12:08	Winter
	17 Jul. 2004	08:12:49	Summer
	24 Aug. 2006	08:13:30	Summer
	10 Jul. 2007	08:14:04	Summer
	03 Dec. 2008	08:13:14	Winter
	04 Jan. 2009	08:13:29	Winter
	31 Jul. 2009	08:14:06	Summer

	21 Jul. 2011	08:17:22	Summer
	24 Aug. 2012	08:19:04	Summer
LandSat8	03 Aug. 2013	08:25:52	Summer
	22 Aug. 2014	08:23:56	Summer

2.2. Meteorological Data

Near surface air temperatures, relative humidity and wind speed for the study area were freely downloaded from Weather Underground website (http://www.wunderground.com/wundermap/). Weather Underground began as an Internet program to display worldwide weather data, developed by University of Michigan in 1991 that officially published in 1995. Data were downloaded for the same date and time of the Landsat data (Table 2).

Figure 2 shows the framework of the methodology adopted in this research. Initially the satellite data was geometrically corrected to the Universe Transverse Mercator (UTM) grid system (WGS, 1984). It has also radiometrically corrected based on the darkest pixel theory [34, 35, 36, 37]. Due to the Landsat sensor has had malfunction since 2003, therefore the data between 2003 and 2012 was having SLC-OFF problem that required GAP-FILL.

Table 2: *List of the Meteorological Data used in this Research*

Date	Min. Air Temperature (℃)	Max. Air Temperature (℃)	Relative Humidity %	Wind Speed (Km/h)
04/08/1990	23	36.4	0.63	19.6
13/08/1999	24	37	0.64	16.8
23/08/2000	21	32	0.55	15.5
30/01/2001	7	23	0.54	8.4
19/12/2002	13	21	0.58	30.8
07/07/2003	25	37	0.60	21.0
17/07/2004	22	32	0.56	16.8
24/08/2006	25	38	0.59	13.8
10/07/2007	23	36	0.61	11.2
03/12/2008	14	27	0.61	16.8
04/01/2009	9	18	0.61	7.1
31/07/2009	24	35	0.65	13.8
21/07/2011	24	37	0.52	14.5
24/08/2012	23	35	0.56	17.5
03/08/2013	24	34	0.59	16.0
22/08/2014	24	36	0.59	14.0

2.3. Image Classification

To correlate the urban heat islands with the existing land cover, supervised classification with maximum likelihood algorithm was used to accurately classify and map the land cover categories. Four major classes were identified namely urban areas, cultivated lands, bare land/desert, and water bodies (Nile River and canals). Road networks were created using on-screen digitizing from high spatial resolution satellite image (IKONOS) to explore the correlation between these infrastructures and the urban heat islands. For further better accuracy, a post classification, technique including adjustments of the categories, was performed to improve the classification outputs.

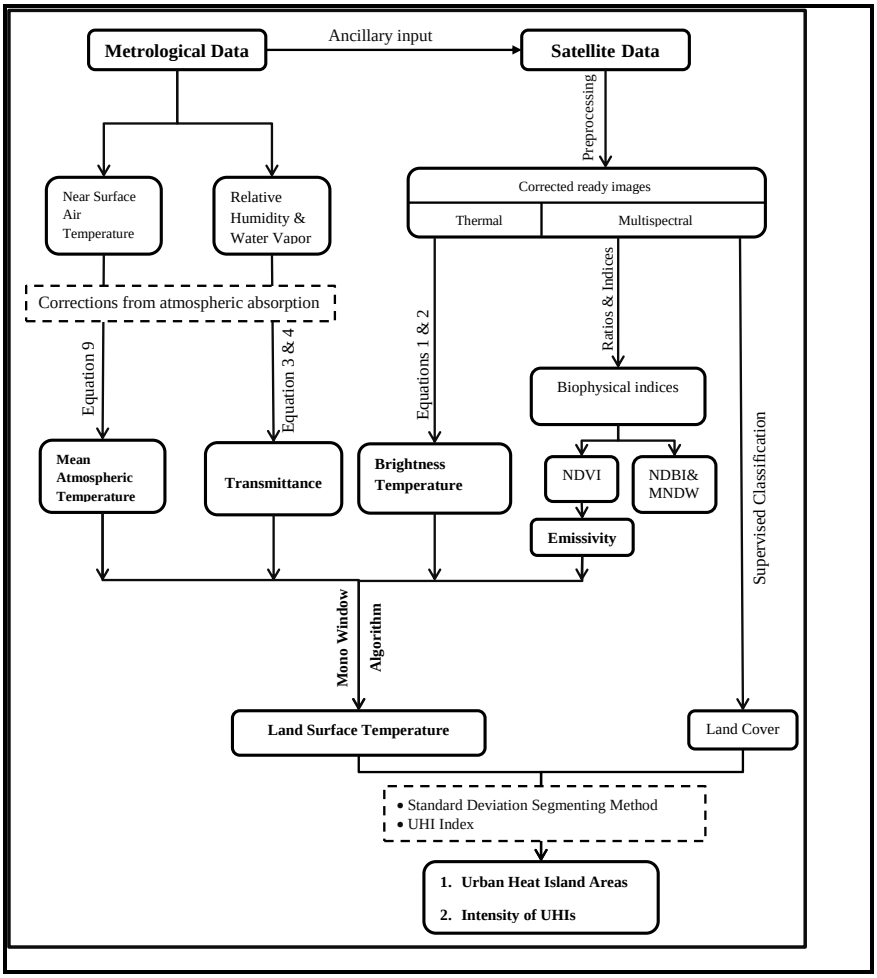

Figure 2: *Framework of the Methodology Approach*

2.4. Mono Window Algorithm for Retrieving Land Surface Temperature

Thermal Infrared in the electromagnetic spectrum ranges between (10.4–12.5 µm), which is covered by the thermal channels of the Landsat series, was used to estimate the at-sensor surface brightness temperature [38, 39, 36, 9, 40].

Figure 2 above shows the framework of the mono-window algorithm to estimate the surface temperature from the thermal infrared channels in combination with other variables and ancillary data. Equations (1 and 2) show the conversion of the DNs (Digital Numbers) to irradiance at sensor and then estimate the brightness temperature from the thermal channels.

$$L_\lambda = L_{min} + \frac{(L_{max} - L_{min})}{(Q_{calmax} - Q_{calmin})}(Q_{calDN} - Q_{calmin}) \qquad \text{Equation (1)}$$

Where:
L_λ = spectral radiance at sensor aperture [W/ (m^2. Sr. µm)],
$L_{MIN\lambda}$ = spectral at-sensor radiance that is scaled to Q_{calmin} or it is the minimum detected spectral radiance [W/ (m^2. Sr. µm)],
$L_{MAX\lambda}$ = spectral at-sensor radiance that is scaled to Q_{calmax} or it is maximum detected spectral radiance [W/ (m^2. Sr. µm)]
Q_{calDN} = quantized calibrated pixel value, represents the Landsat thermal band digital number (DN) values,

Q_{calmin} = the minimum quantized calibrated pixel value corresponding to $L_{MIN\lambda}$,
Q_{calmax} = the maximum quantized calibrated pixel value corresponding to $L_{MAX\lambda}$.

$$T_b = \frac{K_2}{\ln(\frac{K_1}{L_\lambda} + 1)} \qquad \text{Equation (2)}$$

Where:-
T_b = effective at-sensor brightness temperature (°K),
K_1 and K_2 are the calibration constants 1 and 2 (are equivalent to each sensor and obtained from the sensor specifications; for example for Landsat 5 “K1=607.76” & “K2=1260.56”),
L_λ = spectral radiance at the sensor's aperture (W/ (m^2. Sr. µm)),

To obtain a sensibly highly accurate Land Surface Temperature (LST) from at-sensor irradiance it is essential to implement some corrections from atmospheric absorption and re-emission; surface emissivity and surface roughness [22]. This includes:

Atmospheric Transmittance

Atmospheric transmittance is an essential input to the mono window algorithm that is estimated from equation (3). It is actually based on two air temperature profiles (High and Low air temperature) in which each temperature profile divided into two scales of water vapor content [41, 42]. The two profiles of High air temperature and Low air temperature were sub-classified into two categories according to the water vapor (i.e. 04-1.6 and 1.6-3.0 g/cm^2), which resulted in two transmittance value for each profile [43].

$$\tau_i = 1.031412 - 0.11536 * W_v \qquad \text{Equation (3)}$$

Where τ_i = atmospheric transmittance and W_v = water vapor content.

Water vapor is the main factor controlling the estimation of atmospheric transmittance, which is estimated from equation (4) after [41, 42].

$$Wv = 0.0981 * \left\{10 * 0.6108 * \exp\left[\frac{17.27*(T_o - 273.15)}{237.3+(T_o - 273.15)}\right] * RH\right\} + 0.1697 \qquad \text{Equation (4)}$$

Where W_v = water vapor content (g/cm^2);
T_o = near-surface air temperature in ˚K (taken from meteorological data)
RH = relative humidity (taken from meteorological data).

Land Surface Emissivity

Land surface emissivity (LSE) is an essential parameter for estimating the corrected land surface temperature. It is estimated from the Normalized Difference Vegetation Index (NDVI) as descripted in [44, 45, 46, 47]. Equation (5) is the basic equation to estimate the NDVI, then it is scaled to three main categories:

$$NDVI = \frac{\rho 4 - \rho 3}{\rho 4 + \rho 3} \qquad \text{Equation (5)}$$

Where ρ_4 and ρ_3 are the reflectance of the near-infrared and red bands

a) NDVI < 0.2: This category considers the pixel as non-vegetated areas (i.e. bare soil or built-up area or desert) and the emissivity is obtained from reflectivity values in the red region.
b) NDVI > 0.5: This category considers the pixel as fully vegetated, and then a constant value for the emissivity is assumed to be 0.99.
c) 0.2 ≤ NDVI ≤ 0.5: This category considers the pixel as mixture of non-vegetated and fully vegetated areas;

Emissivity is calculated according to the following equation (6):

$$\varepsilon = \varepsilon_v F_v + \varepsilon_u(1-F_v) + d\varepsilon \qquad \text{Equation (6)}$$

Where ε_v = emissivity of vegetation,
ε_u = emissivity of non-vegetated surface (in this study it was used as the emissivity of built-up surface),
F_v = Fractional vegetation cover that computed from the equation (7):

$$Fv = \left(\frac{NDVI - NDVI_{min}}{NDVI_{max} - NDVI_{min}}\right)^2 \qquad \text{Equation (7)}$$

Where $NDVI_{max}$ and $NDVI_{min}$ are the NDVI values in complete vegetation cover region and no vegetation cover region which considered as 0.5 and 0.2 respectively.

The term dε in equation (6) includes the effect of the geometrical distribution of the natural surfaces and also the internal reflections. For plain surfaces, this term is negligible, but for heterogeneous and rough surfaces, as built-up areas, this term can reach a value of 2% [48]. A good approximation for this term can be estimated from equation (8)

$$d\varepsilon = (1-\varepsilon_u)(1-F_v)F\varepsilon_v \qquad \text{Equation (8)}$$

Where F is a shape factor whose mean value is 0.55, considering different geometrical distributions [49].

Mean Atmospheric Temperature

Mean atmospheric temperature is also a main parameter for estimating surface temperature from the Mono Window Algorithm. It was retrieved according to different global weather profile regions using Equation (9).

$$T_a = 16.0110 + 0.92621 * T_o \qquad \text{Equation (9)}$$

Where T_a is the mean atmospheric temperature, T_o is the near-surface air temperature (°K)

Estimation of Land Surface Temperature

In order to estimate the final Land Surface Temperature in the area of study a spatial model was developed using the ArcGIS package based on the mono window algorithm. The three following equations were the main drivers of this model to estimate LST.

$$T_s = \{a(1-C-D) + [b(1-C-D) + C + C]Tb - DTa\}/C \qquad \text{Equation (10)}$$

$$C = \varepsilon i * \tau i \qquad \text{Equation (11)}$$

$$D = (1-\tau i)[1 + (1-\varepsilon i) * \tau i] \qquad \text{Equation (12)}$$

a = -67.355351
b = 0.458606

Where T_s is the LST (°K); (a and b) are constant values; T_b is the brightness temperature (˚K) which was obtained from equation (2); τ_i is the atmospheric transmittance, which was computed from equation (3); ε_i is the land surface emissivity which was either retrieved from equation (6) or got a constant value; and finally T_a represents the effective mean atmospheric temperature, which was applied using equation (9).

Finally in order to convert LST from degree Kelvin to degree Celsius, the following formula was used:

$$Ts\ (°C) = Ts\ (°K) - 273.15 \qquad \text{Equation (13)}$$

Extraction of Heat Island Areas

Heat Island Areas (HIAs) reflect the spatial extent of Urban Heat anomaly. It actually estimated from land surface temperature by segmenting the urban surface temperatures from LST images. Standard deviation segmenting method was used to extract both the hot and cold islands by determining a threshold from the standard deviation of the surface mean temperature [50, 40, 43].

The principle of standard deviation segmenting method is to calculate values of threshold for each element of statistical series based on arithmetic mean and standard deviation of LST image using equation (14);

$$T = a \pm \chi * sd \qquad \text{Equation (14)}$$

Where (T) represents the temperature threshold value, (a) is the mean value of the surface temperature for the area of study, χ (χ = -3, -2.5, -2, -1.5, -1, 0, -0.5, 0.5, 1, 1.5, 2, 2.5, 3) is the times of standard deviation, while Sd is the standard deviation of LST image. Here thirteen values were prepared for χ and thirteen temperature threshold scales were calculated according to different values of χ ranging from –3 to 3 by the interval of 0.5.

To precisely locate either the urban heat islands or the urban cool islands; the LST is classified into 13 slices (levels), which are then isolated using the mean LST +1 Stdv (to map the urban heat islands) and the mean LST -1 Stdv (to map the urban cool islands)

Urban Heat Islands Intensity Index (UHI Index)

The UHIs intensity index is a method to determine the spatial distribution of UHIs intensity [51]. In this research UHIs index was estimated using equation (15). The output is always scaled to 5 categories from extreme strong heat islands to weak heat islands. This will be illustrated in the result section.

$$T_r = \frac{T_i - T_a}{T_a} \qquad \text{Equation (15)}$$

Where, T_r is the relative LST, T_i is LST at one site and T_a is the average LST.

Estimation of Normalized Difference Build-up Index (NDBI)

Normalized Difference Build-up Index (NDBI) is one of the widely used indices to precisely isolate the built-up areas [52]. The development of the index was based on the unique spectral response of built-up lands that have higher reflectance in MIR wavelength range than in NIR wavelength range [53]. In this research the NDBI was estimated using equation (16) [8].

$$NDBI = \frac{MIR - NIR}{MIR + NIR}$$ Equation (16)

Where, MIR and NIR are the middle infrared and the near-infrared bands of Landsat data, respectively.

Estimation of Modified Normalized Difference Water Index (MNDWI)

The Modified Normalized Difference Water Index was used to delineate open water features, which depends mainly on the higher reflectance in the green light wavelength and lower reflectance of MIR [53]. This index was estimated using equation (17).

$$MNDWI = \frac{G - MIR}{G + MIR}$$ Equation (17)

Where, MIR is a middle infrared band and G is Green band of Landsat data.

3. Results and Discussion

3.1. Land Cover Changes

Key element of studying the heat islands in big cities is to understand the changes of land cover. Table 3 lists the land cover changes in the last 24 years showing significant growth of the urbanized area. Such changes are analyzed to be correlated against the surface temperature and urban heat islands. The category of urban areas is merged with the road infrastructures due to they have similar behave in heat emission.

Table 3: *Land Cover Categories and their Changes in the Last 24 Years*

Class/	Area (km^2)		Changes	
	1990	2014	Area (km^2)	%
Urban areas	290.0	436.5	+ 146.4	16.6
Cultivated lands	196.6	172.6	- 24.1	-2.7
Water bodies	15.4	15.0	- 0.5	-0.1
Bare land/ Desert	381.5	259.6	- 121.9	-13.8
Total	883.6	883.6	0	0

3.2. Land Surface Temperature

The retrieved Land Surface Temperature (LST) from Landsat thermal channels for the summer of 1990 and 2014 shown in Figure (3-A and 3-B). Field observations and site visits aided in correlating the LST against the land cover categories, which indicated that the industrial estates, residential areas, development areas and bare land/ desert are places with the highest surface temperature compared with other categories of vegetation and water bodies. It was observed that northwestern and southwestern suburbs such (e.g. Qalyob, El-Qanater El-Khairia and Al-Giza districts), except the built-up areas, showed lower surface temperatures than eastern side with new built-up cities (e.g. Al-Obour, Al-Shrouk and New Cairo) and city center areas (e.g. Old Egypt, Nasser City, etc.). This could be explained that the surroundings of the new built-up areas in the eastern side are mostly desert landscape that accelerates heat advection and convection; however the other sides are fully surrounded with agriculture that cool down the surface temperature.

The large population density in old urban areas which increase the human activities and the percent of waste with heat emissions, play also a role in increasing LST in urban areas as pointed by [54]. For example (annotated in Figure 3), “Old Egypt district” that shows high LST, its population density is 22352 inhabitant/km^2 compared with “El-Zamalek” district that shows lower LST and population of 6450 inhabitant/km^2 [55].

Road networks in built up areas contribute to the thermal heat advection and showed also high surface temperature due to the impervious covering material (e.g. asphalt and concrete) [31]. In this context, in our research study area the road networks coupled with the heavy traffic of up to 4 million transportation vehicles has shown high anomaly of LST that nearly 10% higher than surroundings (Figure 4).

Fundamentally, the variation in LST in built-up areas returns to some essential factors: 1) building material (brick, concrete); 2) street canyons; 3) solar radiation and 4) sun elevation. To recognize this influence of these parameters, a cross section (A - B) in the NW-SE direction of about 40 Km length in the summer of 2000 is analyzed (Figure 5). The profile shows oscillation of LST that ranged from lower values in densely vegetated areas in the north region of Cairo to higher values in densely urbanized areas in Cairo city center as well as near the desert land in the south (above 50°C in summer). There is high anomaly in the middle of the curve, which is signposted by the letter (H) returns to the effect of the factories in area of Al-Ameria (industrial estate); while the observed low area of LST which is signposted by the letter (C) is due to the effect of green area in “Kids Park” in Nasser City district. This could explain the high presence of LST with human activities and anthropogenic emissions from industrial estates at Al-Ameria and Shoubra El-Kheima.

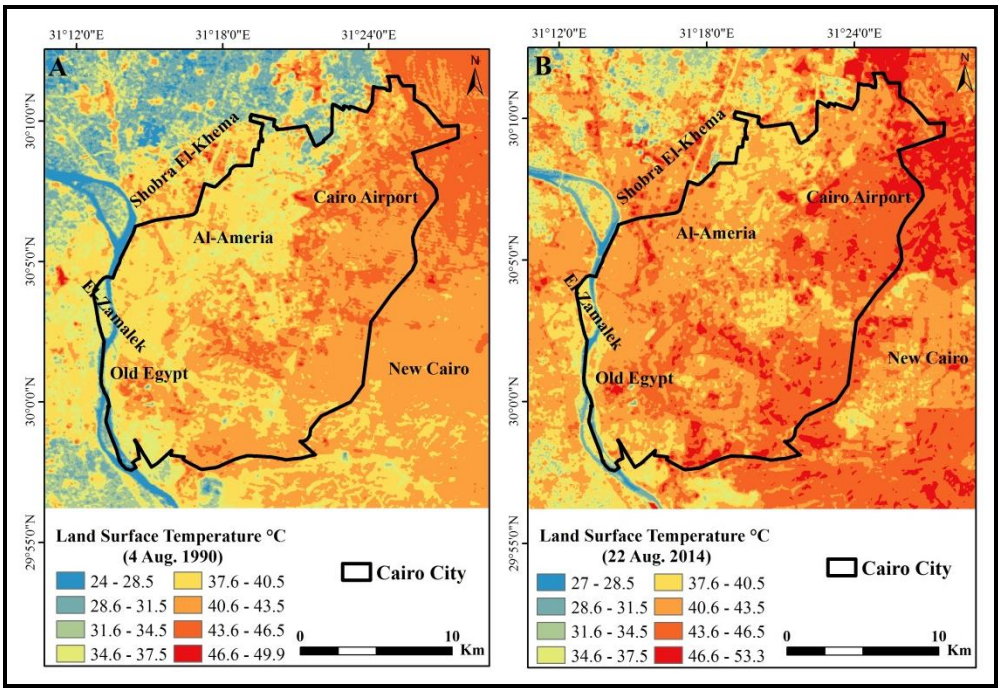

Figure 3: *The Spatial Distribution of LST in °C (A summer of 1990 and B summer of 2014*

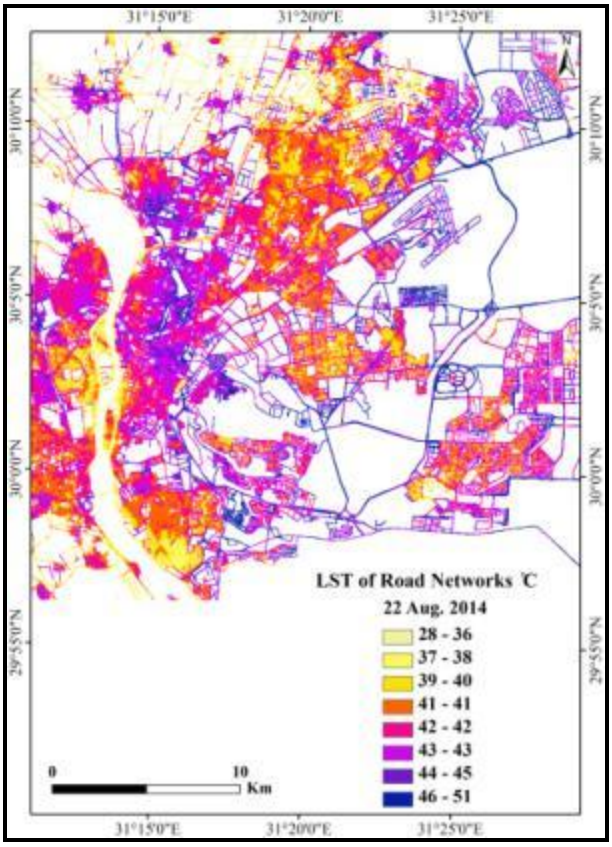

Figure 4: *LST of Road Networks in summer 2014 in °C*

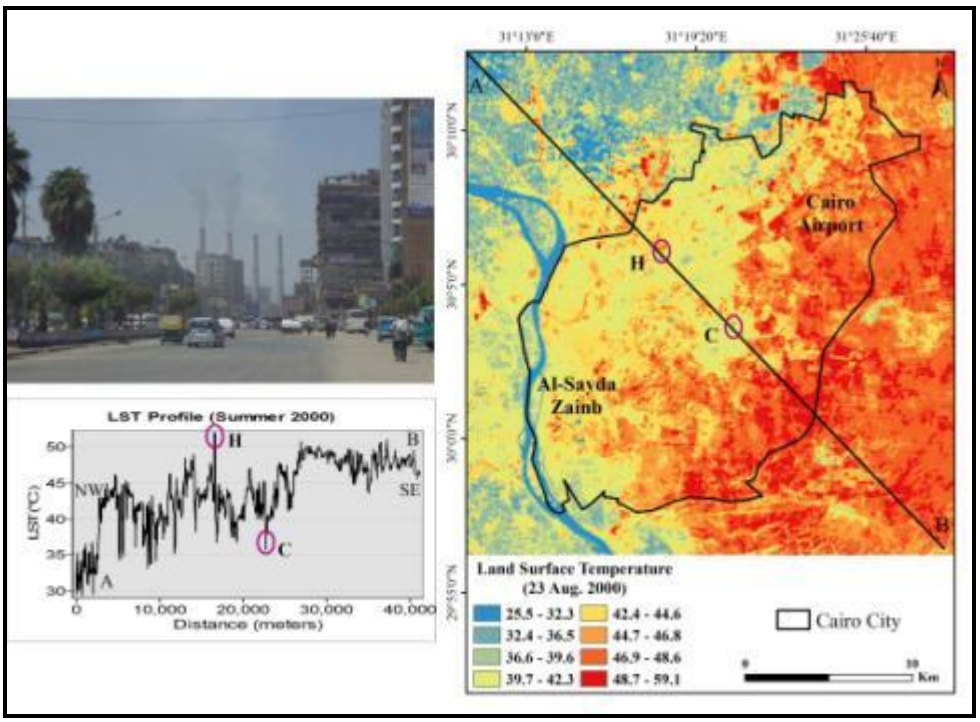

Figure 5: *LST Profile for Shubra El-Kheima Industrial area in summer 2013*

The trend line of the estimated LST (from 1990 to 2014) shows an increase of the summer temperature (Figure 6). In 1990 LST was ranged from minimum of 24 °C to a maximum of 49.9 °C;

however, in 2014 was ranged from minimum of 27 °C to a maximum of 53.3 °C. The slope of the LST increase in this period is projecting an increase of 2.5 °C by the end of this century, which is nearly agreeable with the global IPCC of global warming scenario of an increase of temperature from 1-2 °C per 100 years [56].

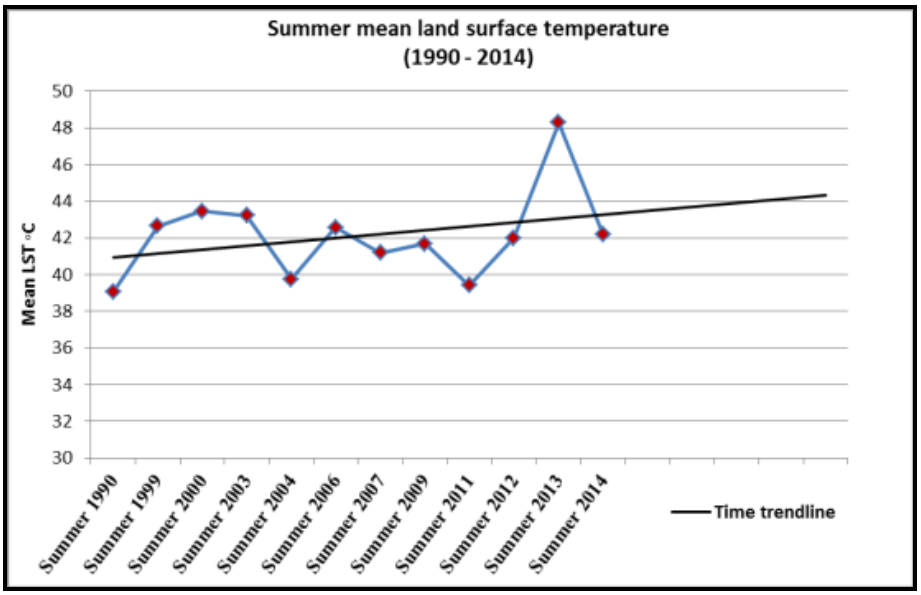

Figure 6: *Slope of the LST Variations in the Last 24 Years*

3.3. Segmentation of Heat Island Areas

Standard deviation segmenting approach was used to isolate the extreme heat islands in the last 24 years (Figure 7A and 7B). Then, it is correlated with land cover to show the direct link between both (Figures 7C). It is observed that most of the high surface temperature zones and heat islands in Cairo were concentrated in densely urbanized and populated areas, industrial zones, transportation networks and bare/desert land, particularly in the densely urbanized and populated city center and the eastern parts of Cairo.

The indirect solar heating and the anthropogenic heat that generated in the urban environment indirectly are the main causes of heat islands. Urban areas generate intense urban canopy heat island areas due to their physical properties including: urban structure, size of the city (population, density of built-up area), ratio of building height to distance with them, width of the streets, building materials, surface materials and sky-view factor.

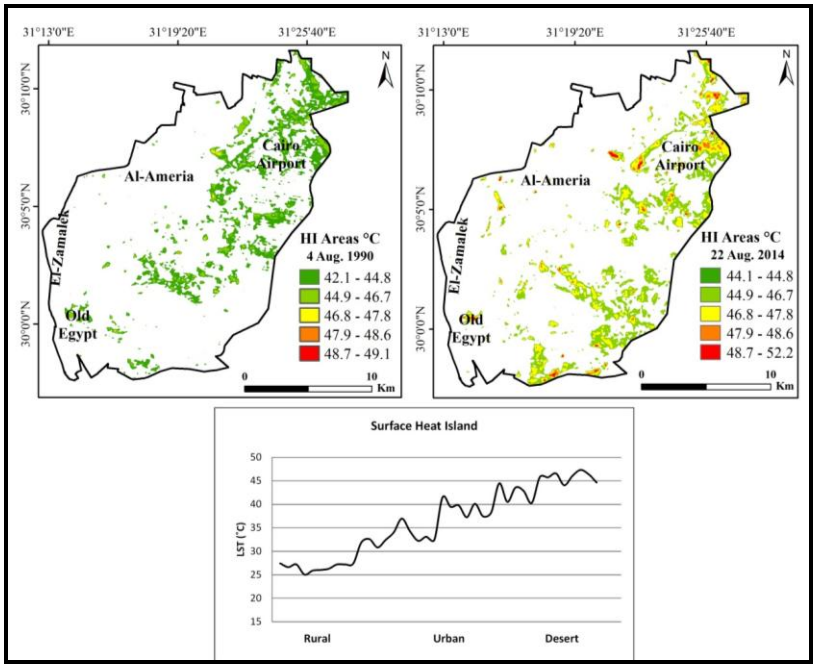

Figure 7: *Comparison of the Intensity of Urban Heat Islands in 1990 and 2014 in Correlation with the Rural and Urbanized Areas*

3.4. Urban Heat Island Intensity

Urban heat island Intensity is determined as the spatially averaged temperature difference between an urbanized and surrounding rural area [57, 58, 59]. The intensity of heat island differs from season to another and modulated by meteorological conditions such as wind speed and cloud cover as well as anthropogenic heat release. Some random observational points of LST values in both urban and rural areas in summer and winter seasons of 2009, for example, were extracted to show the intensity of UHIs in both seasons Figure (8 A&B). In summer the intensity was about 6.6°C while in winter it was about 1.7°C; surface UHIs in winter are much lower in magnitude and smaller in spatial extent than in summer which is agreed with [13]. As shown in Table 4 the difference between mean temperatures of urbanized and surrounding rural areas was 6.6°C, 7.9°C and 10.7°C in summer times of 1990, 2003 and 2013, respectively.

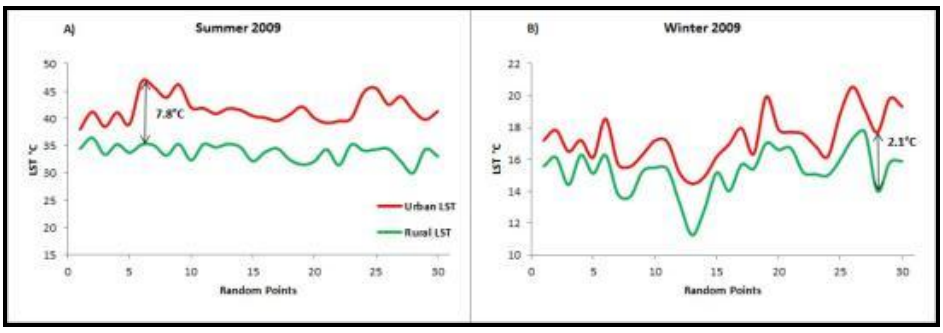

Figure 8: *Variation of Heat Islands Intensity in Urbanized and Rural Areas in Summer and Winter 2009*

Table 4: *Estimated Surface Urban Heat Islands Intensity in (°C)*

Date	Mean Urban LST (°C)	Mean Rural LST (°C)	UHI Intensity (°C)
4 Aug. 1990	39.9	33.3	6.6
7 Jul. 2003	44.3	36.4	7.9
3 Aug. 2013	48.7	38	10.7

The spatial variability of UHIs over Cairo City was estimated using the UHI Index that showed that there are five dominant intensity levels (Figure 9):

a) Level 1: less than 0, this level is considered as a very week HI (green islands). This level occupies the western side of the study area with dominance of vegetation cover (Close to the Nile Delta agriculture land) and water mass (River Nile).
b) Level 2: between 0 and 0.1, this level is considered as weak HI.
c) Level 3: between 0.1 and 0.2, this level is considered as medium heat island. This level often occupies the eastern parts of Cairo.
d) Level 4: between 0.2 and 0.4, this level is considered as a strong HI. This level found in the eastern side and in areas near "Imbaba" airport, and some parts near industrial zones.
e) Level 5: more than 0.4, it is considered as extremely strong HI. This level found in some small scattered bare land areas and industrial estates.

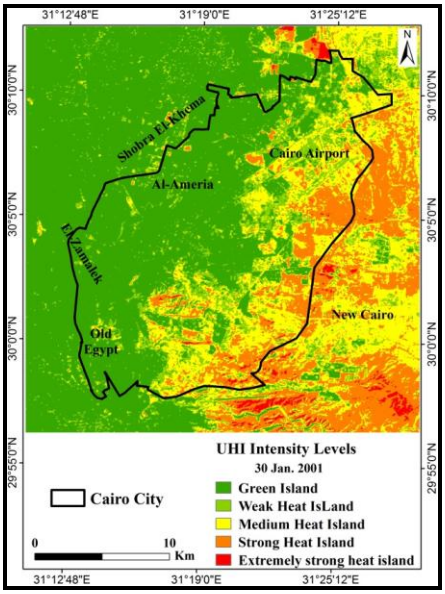

Figure 9: *Example of the Spatial Variability of UHII over Cairo districts in winter 2002*

Table 5 lists the area coverage and statistical analysis of the seasonal UHIs in the last 24 years. The maximum LST in 1990 was in the range of 48- 49.14°C that occupied a small area of nearly 0.03 km^2. However, in 2014 the maximum LST was in the range from 50- 52.2°C that occupied an area of 0.08 km^2. This indicates for an increase in the temperature by about 2°C and in the area by about 0.05 km^2. This table reflects that the maximum area of UHIs was in the summer (August) of 2012 was 65 km^2 with a maximum temperature of 55.7°C. Alternatively; the maximum temperature in the summer (August) was 58.3°C in the summer of 2013 that occupied an area of 36.1 km^2.

The magnitude and extent of UHIs were found highly positively correlated to population size of the cities, indicating the significant impacts of urban growth on the UHI problem. It was also found that the

spatial variability of UHIs in Cairo city was a function of urban surface properties, which in turn was characterized by land covers, most importantly, by vegetation cover and built-up density. The relationship between surface properties and UHIs, confirmed the importance of vegetation and in some degree, urban density in the partition of sensible and latent heat fluxes in humid environment of Cairo city.

Table 5: *UHIs Intensities and Area Coverage in Cairo City in the Last 24 Years*

Season	Date	Cairo City	Statistics			
		HIA (Km^2)	Min.	Max.	Mean	Standard deviation
Summer	04 Aug. 1990	47.3	42.1	49.1	44.2	0.66
	13 Aug. 1999	47.9	45.6	53.0	48.2	0.64
	23 Aug. 2000	47.0	45.7	54.6	49.0	0.72
	07 Jul. 2003	58.1	44.2	52.8	47.9	0.84
	17 Jul. 2004	45.0	39.0	53.3	44.4	1.03
	24 Aug. 2006	53.5	43.5	56.3	47.3	0.93
	10 Jul. 2007	59.0	41.1	51.7	45.3	0.89
	31 Jul. 2009	54.2	41.3	54.7	46.6	0.89
	21 Jul. 2011	48.3	39.7	53.9	44.3	1.1
	24 Aug. 2012	65.0	41.7	55.7	46.6	0.98
	03 Aug. 2013	36.1	50.8	58.3	53.4	0.66
	22 Aug. 2014	55.6	44.0	52.2	46.6	0.73
Winter	30 Jan. 2001	51.2	22.5	35.9	27.5	1.2
	19 Dec. 2002	63.8	17.8	25.5	21.0	0.7
	03 Dec. 2008	66.4	23.9	34.0	27.9	0.96
	04 Jan. 2009	39.9	16.4	27.2	20.3	0.85

3.5. Correlation between Land Surface Temperature and Bio-Physical Indices

A correlation analysis between UHIs and set of bio-physical indices including: Normalized Difference Vegetation Index (NDVI), which indicates green areas; Normalized Difference Build-up Index (NDBI), which represents the build-up land; and Modified Normalized Difference Water Index (MNDWI) which indicates water surfaces and land surface temperature. This correlation was performed in order to compare the different effects of vegetation, build-up areas and water bodies on surface temperature variation and heat islands formation. About 100 points were selected randomly form the LST images and correlated with its corresponding values of NDVI, NDBI, MNDWI (Figure 10 & Table 6). The correlation coefficient “r” ranges between -0.53 and -0.9 for (NDVI), from -0.58 to -0.93 for (MNDWI), and from 0.55 to 0.93 for (NDBI). These correlation coefficients “r” were evaluated by Ramadan [60] as follow: 0.0 (no); 0.3-0.5 (low); 0.5-0.7 (medium); 0.7-0.9 (high); 0.9-1 (very high). So, it is clear that LST had medium to very high negative correlation with both of NDVI and MNDWI. This indicated that the impacts of green land or water bodies on surface temperature is negative and lead to decrease the probability of occurrence of heat islands. This is good indication that green land can reduce the heat islands effect and could be used as a method of mitigation or reduction of heat islands. Conversely, there was a medium to highly significant positive correlation between LST and NDBI which indicates that the built-up land and impervious surfaces can maximize the heat islands effect and increase the probability of urban heat islands formation as proved by Liu and Zhang [8]. It was also found that horizontal expansion of urban has less impact on the presence of UHIs on the fringes of the city and the newly developed suburbs rather than the vertical expansion with high population density and high traffic in the city Centre.

Table 6: *Correlation Coefficient (r) between LST and Bio-Physical Indices*

Date	Correlation Coefficient (r) between		
	LST and NDVI	LST and NDBI	LST and MNDWI
04 Aug. 1990	-0.90	0.93	-0.91
13 Aug. 1999	-0.83	0.90	-0.92
23 Aug. 2000	-0.86	0.87	-0.86
30 Jan. 2001	-0.71	0.72	-0.86
19 Dec. 2002	-0.79	0.75	-0.83
07 Jul. 2003	-0.85	0.86	-0.81
17 Jul. 2004	-0.75	0.82	-0.82
24 Aug. 2006	-0.64	0.85	-0.83
10 Jul. 2007	-0.76	0.79	-0.73
03 Dec. 2008	-0.76	0.67	-0.83
04 Jan. 2009	-0.56	0.55	-0.65
31 Jul. 2009	-0.53	0.81	-0.93
21 Jul. 2011	-0.64	0.77	-0.73
24 Aug. 2012	-0.67	0.76	-0.85
03 Aug. 2013	-0.87	0.91	-0.73
22 Aug. 2014	-0.82	0.85	-0.86

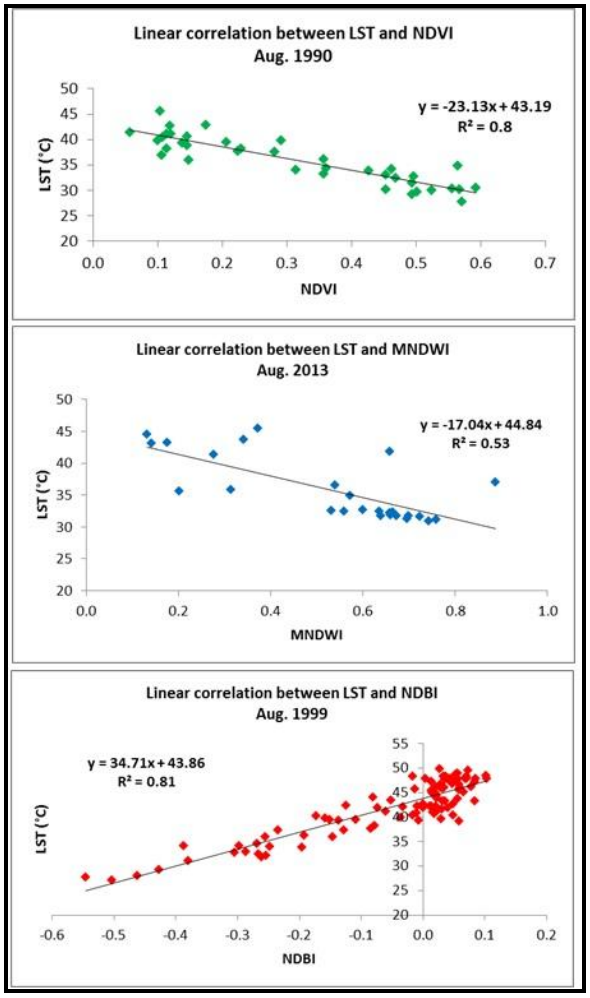

Figure 10: *Correlation between UHIs and Bio-Physical Indices*

4. Conclusion

This study has demonstrated the use of thermal remote sensing from time series of Landsat satellite to well-understand and map the intensity and variability of UHIs in Cairo and the main drivers in the last 24 years. Most of the previous studies on urban heat islands in Cairo and the surrounding areas have been either limited to few *in-situ* observations, or limited to small geographical coverage or limited to narrow time dimension. This study attempted to fill in the gaps and overcome these shortcomings. It is attempted to use readily available freely accessed high temporal resolution of Landsat images to monitor, assess and map urban climates in a mega city "Cairo" and create wide area coverage with wide time dimension of 24 years.

UHIs patterns and its seasonal variation in both intensity and spatial extent over Cairo demonstrated that the driving forces of land cover dynamics and socioeconomic showed high correlation with an enormous increase of LST with dense urbanization, higher population density and industrial activities. It was found that the extreme UHIs inner the city was in the industrial estates of Al-Ameria due to the building materials and emission. Indeed, such understanding and findings could help urban planners and decision-makers to consider such correlation to plan for mitigation and reduction of the LST.

Spatially, there were significant LSTs gradients from the city center and urbanized areas to the surrounding rural areas. This was observed in the correlation with bio-physical indices. The recently emerging urbanizing area and the intensive industrial estates inside the city and at the urban fringe exhibited higher LSTs and remarkable variation in LSTs. Conversely, the surrounding rural areas to the west and northwest exhibited lower LSTs and relative lower variation in LSTs. Moreover, there were significant relationships between LST and fractional vegetation cover, population density, and road density.

It could be concluded that the Landsat data has provided useful free access information for studying UHIs. Understanding the global climate changes phenomena requires more comprehensive data to the city level that would enable to project the implications on human being. This has challenged us to integrate this study in the Global Earth Observation System of Systems (GEOSS) to enable for global integration, comparison and modelling. Future work is needed to improve uncertainties using in-situ data from meteorological station networks and air quality monitoring stations to provide more understanding of the process and mechanism of UHIs associated with LULC and the air quality. However, further studies in the detailed LST–urban surface relationship addressing the urban morphology and air quality in big cities such as Cairo is necessary in order to have insights into the genesis of the surface UHIs and its linkage with the air quality and urban health environment.

References

[1] Giannaros, T.M. and Melas, D. *Study of the Urban Heat Island in a Coastal Mediterranean City: The Case Study of Thessaloniki, Greece.* Atmospheric Research. 2012. 118; 103-120.

[2] Stathopoulou, M. and Cartalis, C. *Daytime Urban Heat Islands from Landsat ETM+ and Corine Land Cover Data: An Application to Major Cities in Greece*. Solar Energy. 2007. 81; 358-368.

[3] Howard, L. *The Climate of London*. London Harvey and Dorton: London, UK. 1833. 2; 1818-1820.

[4] Schwarz, N., Lautenbach, S. and Seppelt, R. *Exploring Indicators for Quantifying Surface Urban Heat Islands of European Cities with MODIS Land Surface Temperatures.* Remote Sensing of Environment. 2011. 115; 3175-3186.

[5] Klysik, K. and Fortuniak, K. *Temporal and Spatial Characteristics of the Urban Heat Island of Łódź, Poland.* Atmospheric Environment. 1999. 33; 3885-3895.

[6] Livada, I., Santamouris, M., Niachou, K., Papanikolaou, N. and Mihalakakou, G. *Determination of Places in the Great Determination of Places in the Great Athens Area Where the Heat Island Effect is Observed.* Theoretical and Applied Climatology. 2002. 71; 219-230.

[7] Miao, S., Chen, F., LeMone, M.A., Tewari, M., Li, Q. and Wang, Y. *An Observational and Modeling Study of Characteristics of Urban Heat Island and Boundary Layer Structures in Beijing.* Journal of Applied Meteorology and Climatology. 2009. 48; 484-501.

[8] Liu, L. and Zhang, Y. *Urban Heat Island Analysis Using the Landsat TM Data and ASTER Data: A Case Study in Hong Kong.* Journal of Remote Sensing. 2011. 1535-1552.

[9] Li, J., Song, C., Cao, L., Zhu, F., Meng, X. and Wu, J. *Impacts of Landscape Structure on Surface Urban Heat Islands: A Case Study of Shanghai, China.* Remote Sensing of Environment. 2011. 115; 3249-3263.

[10] Emmanuel, R. and Krüger, E. *Urban Heat Island and Its Impact on Climate Change Resilience in a Shrinking City: The Case of Glasgow, UK.* Building and Environment. 2012. 53; 137-149.

[11] Schwarz, N., Schlink, U., Franck, U. and Grobmann, K. *Relationship of Land Surface and Air Temperatures and its Implications for Quantifying Urban Heat Island Indicators–An Application for the City of Leipzig (Germany).* Ecological Indicators. 2012. 18; 693-704.

[12] Kato, S. and Yamaguchi, Y. *Analysis of Urban Heat–Island Effect Using ASTER and ETM+ Data: Separation of Anthropogenic Heat Discharge and Natural Heat Radiation from Sensible Heat Flux.* Remote Sensing of Environment. 2005. 99; 44-54.

[13] Hung, T., Uchihama, D., Ochi, S. and Yasuoka, Y. *Assessment with Satellite Data of the Urban Heat Island Effects in Asian Mega Cities.* International Journal of Applied Earth Observation and Geoinformation. 2006. 8; 34-48.

[14] Oke, T.R., 1987: *Boundary Layer Climates.* Second Edition, Methuen, London, New York. 262-330.

[15] Gallo, K.P., McNab, A.L., Karl, T.R., Brown, J.F., Hood, J.J. and Tarpley, J.D. *The Use of NOAA AVHRR Data for Assessment of the Urban Heat Island Effect.* Journal of Applied Meteorology. 1993. 32; 899-908.

[16] Gallo, K.P. and Owen, T.W. *Assessment of Urban Heat Island: A Multi-Sensor Perspective for the Dallas-Ft. Worth, USA Region.* Geocarto International Journal. 1998. 13; 35-41.

[17] Dousset, B. and Gourmelon, F. *Satellite Multi-Sensor Data Analysis of Urban Surface Temperatures and Land Cover.* ISPRS Journal of Photogrammetry and Remote Sensing. 2003. 58; 43-54.

[18] Roth, M., Oke, T.R. and Emery, W.J. *Satellite– Derived Urban Heat Islands from 3 Coastal Cities and the Utilization of Such Data in Urban Climatology.* International Journal of Remote Sensing. 1989. 10 (11) 1699-1720.

[19] Streutker, D.R. *A Remote Sensing Study of the Urban Heat Island of Houston, Texas.* International Journal of Remote Sensing. 2002. 23 (13) 2595-2608.

[20] Streutker, D.R. *Satellite–Measured Growth of the Urban Heat Island of Houston, Texas.* Remote Sensing of Environment. 2003. 85; 282-289.

[21] Weng, Q., Lu, D. and Schubring, J. *Estimation of Land Surface Temperature, Vegetation Abundance Relationship for Urban Heat Island Studies.* Remote Sensing of Environment. 2004. 89 (4) 467-483.

[22] Voogt, J.A. and Oke, T.R. *Thermal Remote Sensing of Urban Climates.* Remote Sensing of Environment. 2003. 86 (3) 370-384.

[23] Zaki, R., Zaki, A. and Ahmed, S. *Land use and Land Cover Changes in Arid Region: The Case New Urbanized Zone, Northeast Cairo, Egypt.* Journal of Geographic Information System. 2011. 3; 173-194.

[24] Bottyán, Z. and Unger, J. *A Multiple Linear Statistical Model for Estimating the Mean Maximum Urban Heat Island.* Theoretical and Applied Climatology. 2003. 75 (3-4) 233-243.

[25] Eliasson, I. *Urban Nocturnal Temperatures, Street Geometry and Land Use.* Atmospheric Environment. 1996. 30 (3) 379-392.

[26] Fan, H. and Sailor, D.J. *Modeling the Impacts of Anthropogenic Heating on the Urban Climate of Philadelphia: A Comparison of Implementations in Two PBL Schemes.* Atmospheric Environment. 2005. 39 (1) 73-84.

[27] Weng, Q., Lu, D. and Liang, B. *Urban Surface Biophysical Descriptors and Land Surface Temperature Variations.* Photogrammetric Engineering and Remote Sensing. 2006. 72 (11) 1275-1286.

[28] Xiao, R., Weng, Q., Ouyang, Z., Li, W., Schienke, E.W. and Zhang, W. *Land Surface Temperature Variation and Major Factors in Beijing, China.* Photogrammetric Engineering and Remote Sensing. 2008. 74 (4) 451-461.

[29] Elvidge, C.D., Baugh, K.E., Kihn, E.A., Kroehl, H.W., Davis, E.R. and Davis, C.W. *Relation Between Satellites Observed Visible–Near Infrared Emissions, Population, Economic Activity and Electric Power Consumption.* International Journal of Remote Sensing. 1997. 18 (6) 1373-1379.

[30] Molina, M.J. and Molina, L.T. *Critical Review: Megacities and Atmospheric Pollution.* Journal of Air Waste Management Association. 2004. 54; 644-680.

[31] Marey, H.S., Gille, J.C., El-Askary, H.M., Shalaby, E.A. and El-Raey, M.E. *Study of the Formation of the "Black Cloud" and its Dynamics Over Cairo, Egypt, Using MODIS and MISR Sensors.* Journal of Geophysical Research. 2010. 115 (D21206) 1-10.

[32] El-Metwally M., Alfaro, S.C., Abdel-Wahab, M.M., Favez, O., Mohamed, Z. and Chatenet, B. *Aerosol Properties and Associated Radiative Effects Over Cairo (Egypt).* Atmospheric Research. 2011. 99; 263-276.

[33] Yin, Z.Y., Stewart, D.J., Bullard, S. and MacLachlan, J.T. *Changes in Urban Built–Up Surface and Population Distribution Patterns during 1986–1999: A Case Study of Cairo, Egypt.* Computers, Environment and Urban Systems. 2005. 29; 595-616.

[34] Chavez, P.S. *Image-Based Atmospheric Correction-Revisited and Improved.* Photogrammetric Engineering and Remote Sensing. 1996. 62; 1025-1036.

[35] Lu, D., Mausel, P., Brondizio, E. and Moran, E. *Assessment of Atmospheric Correction Methods for Landsat TM Data Applicable To Amazon Basin LBA Research.* International Journal of Remote Sensing. 2002. 23 (13) 2651-2671.

[36] Chander, G., Markham, B.L. and Helder, D.L. *Summary of Current Radiometric Calibration Coefficients for Landsat MSS, TM, ETM+, and EO–1 ALI Sensors.* Remote Sensing of Environment. 2009. 113 (5) 893-903.

[37] Li, Y., Zhang, H. and Kainz, W. *Monitoring Patterns of Urban Heat Islands of the Fast-Growing Shanghai Metropolis, China: Using Time-series of Landsat TM/ETM+ Data.* International Journal of Applied Earth Observation and Geoinformation. 2012. 19; 127-138.

[38] Barsi, J.A., Schott, J.R., Palluconi, F.D., Helder, D.L., Hook, S.J. and Markham, B.L., Chander, G. and O'Donnell, E.M. *Landsat TM and ETM+ Thermal Band Calibration.* Canadian Journal of Remote Sensing. 2003. 29 (2) 141-153.

[39] Chander, G. and Markham, B. *Revised Landsat-5 TM Radiometric Calibration Procedures and Post Calibration Dynamic Ranges.* IEEE Transactions on Geo–science and Remote Sensing. 2003. 41 (11) 2674-2677.

[40] Zhang, J. and Wang, Y. *Study of the Relationships between the Spatial Extent of Surface Urban Heat Islands and Urban Characteristic Factors Based on Landsat ETM+ Data.* Sensors. 2008. 8; 7453-7468.

[41] Sun, Q., Tan, J. and Xu, Y. *An ERDAS Image Processing Method for Retrieving LST and Describing Urban Heat Evolution: A Case Study in the Pearl River Delta Region in South China.* Environmental Earth Sciences. 2010. 59; 1047-1055.

[42] Qin, Z., Karnieli, A. and Berliner, P.A. *Mono–Algorithm for Retrieving Land Surface Temperature from Landsat TM Data and Its Application to the Israel–Egypt Border Region.* International Journal of Remote Sensing. 2001. 18; 583-594.

[43] Zhang, J., Wang, Y. and Wang, Z. *Change Analysis of Land Surface Temperature Based on Robust Statistics in the Estuarine Area of Pearl River (China) from 1990 to 2000 by Landsat TM/ETM+ Data.* International Journal of Remote Sensing. 2007. 28 (10) 2383-2390.

[44] Griend, A.A. and Owe, M. *On the Relationship between Thermal Emissivity and the Normalized Difference Vegetation Index for Natural Surfaces.* International Journal of Remote Sensing. 1993. 4 (6) 1119-1131.

[45] Valor, E. and Caselles, V. *Mapping Land Surface Emissivity from NDVI: Application to European, African and South American Areas.* Remote Sensing of Environment. 1996. 57; 167-184.

[46] Sobrino, J.A. and Raissouni, N. *Toward Remote Sensing Methods for Land Cover Dynamic Monitoring Application to Morocco.* International Journal of Remote Sensing. 2000. 21; 353-366.

[47] Sobrino, J.A., Jiménez–Muñoz, J.C. and Paolini, L. *Land Surface Temperature Retrieval from LANDSAT TM 5.* Remote Sensing of Environment. 2004. 90 (4) 434-440.

[48] Sobrino, J.A., 1989: Desarrollo de un modelo teo´rico para implementar la medida de la temperatura realizada mediante teledeteccio´n. Aplicacio´n a un campo de naranjos, PhD dissertation, University of Valencia, Valencia, Spain, 170.

[49] Sobrino, J.A., Caselles, V. and Becker, F. *Significance of the Remotely Sensed Thermal Infrared Measurements Obtained over a Citrus Orchard.* ISPRS Journal of Photogrammetry and Remote Sensing. 1990. 44 (6) 343-354.

[50] Rhinane, H., Hilali, A., Bahi, H. and Berrada, A. *Contribution of Landsat TM Data for the Detection of Urban Heat Islands Areas Case of Casablanca.* Journal of Geographic Information System. 2012. 4; 20-26.

[51] Xu, L.Y., Xie, X.D. and Li, S. *Correlation Analysis of the Urban Heat Island Effect and the Spatial and Temporal Distribution of Atmospheric Particulates Using TM Images In Beijing.* Environmental Pollution. 2013. 178; 102-114.

[52] Lu, Y., Feng, P., Shen, C. and Sun, J., 2009: *Urban Heat Island in summer of Nanjing Based on TM Data.* In Proceedings of 2009 Joint Urban Remote Sensing Event, Shanghai, China, 20-22 May. 1-5.

[53] Xu, H. *Extraction of Urban Built up Land Features from Landsat Imagery using a Thematic–Oriented Index Combination Technique.* Photogrammetric Engineering and Remote Sensing. 2007. 73 (12) 1381-1391.

[54] Shangming, D. and Bo, D., 2001: Analysis of the Effects of Urban Heat Islands by Satellite Remote Sensing. Asian Conference of Remote Sensing, 5-9 November, Singapore.

[55] Central Agency for Public Mobilization and Statistics, 2013: The Annual Statistical Book, Egypt, CAPMAS, 332.

[56] International Panel of Climate Change (IPCC), 2007: *Summary for Policymakers*. In: Solomon, S., Qin, D.; Manning, M.; Chen, Z.; Marquis, M.; Averyt, K.B.; Tignor, M. and H.L. Miller (eds.). Climate Change 2007: The Physical Science Basis. Contribution of Working Group I to the Fourth Assessment Report of the Intergovernmental Panel on Climate Chang, Cambridge University Press: Cambridge, United Kingdom and New York, USA, 327.

[57] Magee, N., Curtis, J. and Wendler, G. *The Urban Heat Island Effect at Fairbanks, Alaska.* Theoretical and Applied Climatology. 1999. 64 (1) 39-47.

[58] Kim, Y.H. and Baik, J.J. *Spatial and Temporal Structure of the Urban Heat Island in Seoul.* 2005. Journal of Applied Meteorology. 44, 591-605.

[59] Memon, R.A., Leung, D.Y.C. and Chunho, L. *A Review on the Generation, Determination and Mitigation of Urban Heat Island.* Journal of Environmental Sciences. 2008. 20; 120-128.

[60] Ramadan, A. *Heavy Metal Pollution and Biomonitoring Plants in Lake Manzala, Egypt*. Pakistan Journal of Biological Sciences. 2003. 6 (13) 1108-1117.